Reconstruction of dynamic wind turbine wake flow fields from virtual Lidar measurements via physics-informed neural networks

Journal of Physics: Conference Series **2767** (2024) 092017 doi:10.1088/1742-6596/2767/9/092017

Reconstruction of dynamic wind turbine wake flow fields from virtual Lidar measurements via physics-informed neural networks

Jincheng Zhang and Xiaowei Zhao

Intelligent Control & Smart Energy (ICSE) Research Group, School of Engineering, The University of Warwick, Coventry CV4 7AL, UK

E-mail: jincheng.zhang.1@warwick.ac.uk; xiaowei.zhao@warwick.ac.uk

Abstract. Accurate characterisation of wind turbine wakes is important for the optimal design and operation of wind farms. However, current techniques for full-scale wind measurements are still limited to point characterisation. To address the research challenge in obtaining field characterisation of real-world wind turbine wakes, this work investigates the reconstruction of the dynamic wake flow fields based on a virtual turbine-mounted Lidar and physics-informed neural networks. Specifically, the wake flow field is reconstructed by fusing the sparse measurements with the two-dimensional Navier-Stokes equations without imposing any models for the unsteady wake. Different from supervised machine learning approaches which need the measured values for the quantities of interest in the first place, the proposed method can achieve the prediction of the wind velocity at new locations where there is no measurement available. The reconstruction performance is evaluated via high-fidelity numerical experiments and it is shown that the dynamic wind turbine wake flow fields are predicted accurately, where the main wake features, including the downwind development and crosswind meandering of the wake, are both captured. This work thus paves the way for investigating full-scale in situ wake flow dynamics in real-world wind energy sites.

1. Introduction

Wind turbine wakes, i.e. the flow regions behind wind turbines where the wind speed is reduced and the turbulence level is increased, are of great importance for the optimal design and operation of wind farms. In order to investigate wake effects, a lot of works have been carried out, ranging from physics-based wake modelling [1, 2, 3, 4], data-driven modelling [5, 6, 7], numerical simulations [8, 9, 10], wind tunnel measurements [11, 12, 13], and field measurement campaign [14, 15, 16]. While many works focus on the theoretical and numerical study of wind turbine wakes, it is still extremely challenging to directly measure the wake flow fields in real-world conditions. Detailed flow measurements, e.g. PIV measurements, can be achieved with model wind turbines in a controlled wind tunnel environment. However, for full-scale wind energy sites, flow field measurements are still limited to sparse spatial locations.

Remote sensing devices, such as turbine-mounted Lidars, are becoming more and more popular for wind energy measurements [17, 18, 19]. They have the potential to provide richer information than traditional wind speed anemometers. The use of Lidar measurements for reconstructing flow fields in the wake regions has also been investigated recently. In [20], two

separate Lidars were employed for predicting wake flow fields and the results showed that the proposed method was able to predict the time-averaged wake flow fields accurately. In [21], scanning Lidars were used for reconstructing steady wind turbine wake flow fields in 3D space, and the results showed that the averaged flow fields were predicted accurately. In [22], the 3D dynamic wake flow fields were predicted, combining long-range Lidar and dynamic wake models. In [23], the wake flow fields in the plane parallel to the turbine rotor were predicted and then they were used for wind turbine load evaluations. The results showed that the main wake features were predicted successfully while the Lidar's resolution was not sufficient for power and load assessments.

Most of the above works showed that more details regarding the wind turbine wake flow fields can be obtained by combining data with physical knowledge (e.g. empirical models). However, due to various assumptions, such as the steady flow assumption, the spatiotemporal variability of the flow fields was constrained accordingly. To address the issue, in this work, the dynamic wake flow field is reconstructed by fusing the measurements of a virtual turbine-mounted Lidar with the two-dimensional Navier-Stokes equations, without analytically modelling the wake while at the same time capturing the dynamic flow features. The employed data-physics fusion approach is based on the physics-informed neural networks (PINNs) [24], which has seen great successes since being proposed [25, 26]. For wind energy applications, PINNs have been employed for the prediction of the freestream atmospheric boundary layer flow [27, 28] and wake interactions [29] lately. This work aims to explore the power of PINNs and Lidar to reconstruct the complex wind turbine wake flows.

The rest of the paper is organised as follows. The wake flow field reconstruction approach is presented in Section 2, including the virtual Lidar setups, PINNs structures, and the numerical simulation details. Then the results are given in Section 3, where the reconstructed flow fields are compared with the corresponding ground truth and the wake profiles and effective wind speeds are extracted for further analysis. Finally the conclusions are drawn in Section 4.

2. Methodology

The wake flow field is reconstructed based on the line-of-sight measurements by a virtual Lidar and the two-dimensional Navier-Stokes (NS) equations via the PINNs approach. In particular, this work focuses on the flow field at the turbine hub height. Therefore, the virtual Lidar is designed to scan over the hub-height 2D plane and the objective of the reconstruction is to retrieve the detailed flow fields in the wake regions at the hub height.

2.1. Lidar setups

The virtual Lidar device in this work, in terms of data frequency and measurement range, is designed based on the product guide of the ZXTM Lidar developed by the ZXLidars [30]. As this work focuses on the flow fields in the turbine hub-height 2D plane, the virtual Lidar device is configured to carry out Plan-Position Indicator (PPI) scan, where multiple positions per laser beam direction are measured simultaneously and the laser beam is set to scan horizontally within the hub-height 2D plane. Such scan pattern is designed following previous works in the literature [22]. Specifically, the measurement points are uniformly distributed along the laser beam direction, from 25 m to 550 m with the distance between adjacent measurement points as 35 m. This leads to a total of 16 measurement points per Lidar-staring direction. The PPI scan is set to be carried out from -15 to 15 degrees, which is sufficient to cover the main wake-influenced regions, and the scanning speed is set as 7.5 degrees per second. Moreover, due to the limitation of data frequency (e.g. 50 data points per second in the case of ZXTM Lidar), the virtual device is designed to scan three PPI directions every second, thus leading to a total of 48 measurement points per second. The overall Lidar setups are illustrated in Figure 1 where all the data points that are covered by a complete scanning cycle are shown.

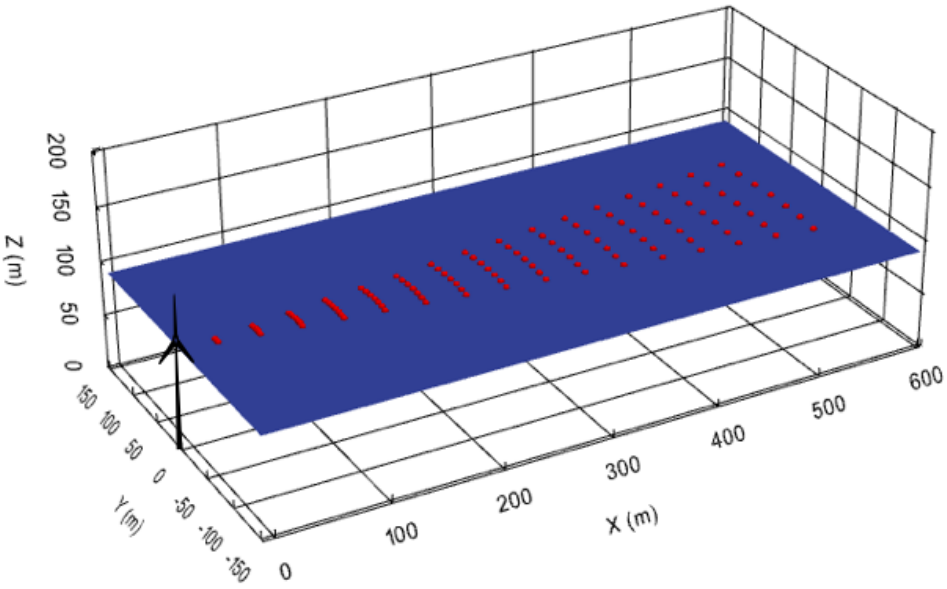

Figure 1. The illustration of the virtual scanning Lidar measurements over the horizontal plane at the turbine hub height.

2.2. PINNs for wake flow reconstruction

The raw measurements by the virtual Lidar contain only the line-of-sight wind speeds at sparse spatial locations. To reconstruct the wake flow fields, flow physics, in the form of either analytical models, simulation data obtained from numerical models, or partial differential equations, must be used to retrieve the missing information not contained in the measurement data. In this work, we employ the physics-informed neural networks (PINNs) approach to incorporate the two-dimensional NS equations in the flow field reconstruction procedure. The overall approach is similar to the works in [27, 28] which focus on the atmospheric flows in front of the wind turbines, while this work focuses on the more complex wake flows behind wind turbines. The overall PINNs structure and its training are briefly described in this section. The interested reader may refer to [27, 28] for further details.

To construct the machine learning model that is informed by both Lidar data and physics, the base neural network (NN) is first constructed, which maps the spatiotemporal coordinates to the flow states. They can be expressed as

$$\mathbf{Y} = \mathcal{N}(\mathbf{X}) \tag{1}$$

where

$$\mathbf{X} = [x, y, t], \mathbf{Y} = [u, v, p] \tag{2}$$

Here x, y, t represent the spatial coordinate in the downwind direction, the spatial coordinate in the crosswind direction, and the time coordinate respectively. u, v, and p represent the wind speed in the downwind direction, the wind speed in the crosswind direction, and the static pressure. The base NN, i.e. $\mathcal{N}$, is specified as a fully-connected neural network in this work and it is parameterised by the trainable weights W which will be updated to minimise the training loss during the training process.

The training loss is designed to be composed of two parts. The first part, which is the supervised part, aims to minimise the mismatch between the predicted flow quantities and the

virtual Lidar measurements. It is defined as

$$\mathbf{L}_1 = \frac{1}{N_1}\sum_{i=1}^{N_1}(u_i^{LoS} - \hat{u}_i^{LoS})^2 \tag{3}$$

Here u_i^{LoS} and $\hat{u}_i^{LoS}$ represent the i^{th} line-of-sight measurement by Lidar and the projection of the corresponding NN output at this time and location in the Lidar direction. The second part, which is the physics-informed part, aims to softly enforce the two-dimensional NS equations at the test points. It is defined as

$$\mathbf{L}_2 = \frac{1}{N_2}\sum_{i=1}^{N_2}(e_i^u)^2 + \frac{1}{N_2}\sum_{i=1}^{N_2}(e_i^v)^2 + \frac{1}{N_2}\sum_{i=1}^{N_2}(e_i^{div})^2 \tag{4}$$

where

$$e^u = \frac{\partial u}{\partial t} + u\frac{\partial u}{\partial x} + v\frac{\partial u}{\partial y} + \frac{\partial p}{\partial x} - \frac{1}{Re}(\frac{\partial^2 u}{\partial x^2} + \frac{\partial^2 u}{\partial y^2})$$

$$e^v = \frac{\partial v}{\partial t} + u\frac{\partial v}{\partial x} + v\frac{\partial v}{\partial y} + \frac{\partial p}{\partial y} - \frac{1}{Re}(\frac{\partial^2 v}{\partial x^2} + \frac{\partial^2 v}{\partial y^2})$$

$$e^{div} = \frac{\partial u}{\partial x} + \frac{\partial v}{\partial y}.$$

Here e^u, e^v, e^{div} are derived using automatic differentiation based on the base NN $\mathcal{N}$. They are evaluated at the randomly chosen test points in the domain of interest to enforce the constraints imposed by the 2D NS equations. Finally, the training of the machine learning model is carried out to minimise the total loss, which is defined as

$$\mathbf{L} = \mathbf{L}_1 + \mathbf{L}_2 \tag{5}$$

Here it is worth mentioning that the overall model is unsupervised from the machine learning perspective. The only data required for training is the LoS wind speed at the sparse measurement locations, while the data for the whole flow fields and other unmeasured quantities such as pressure are not needed.

2.3. Numerical experiments

In this work, the high-fidelity numerical simulation solver SOWFA [31] is used to serve as the platform to carry out the numerical experiments. The main reason of using numerical experiments for evaluating the reconstruction performance is that the ground truth for the full flow fields is available. While in real-world wind energy sites, even though the wind field can be reconstructed once the Lidar device is installed in place, the evaluation of the reconstruction accuracy remains a great challenge. In our future work, we will explore the use of wind tunnel experiments for method evaluations, where the ground truth will be captured by detailed PIV measurements. This work thus also serves as a guidance for future experimental works, providing insights on measurement configurations and neural network specifications.

Particularly, in this paper, the neutral atmospheric boundary layer is considered for the large eddy simulations of wind turbine wakes. The freestream mean wind speed is set as 8 m/s and the freestream turbulence intensity is set as 6%. The bottom boundary is handled by the surface stress and temperature flux model as well as zero normal velocity, the top boundary is imposed with zero stress and temperature flux as well as zero normal velocity, and the cyclic condition is imposed for the lateral boundaries [32]. The NREL 5MW reference turbine [33] is modelled

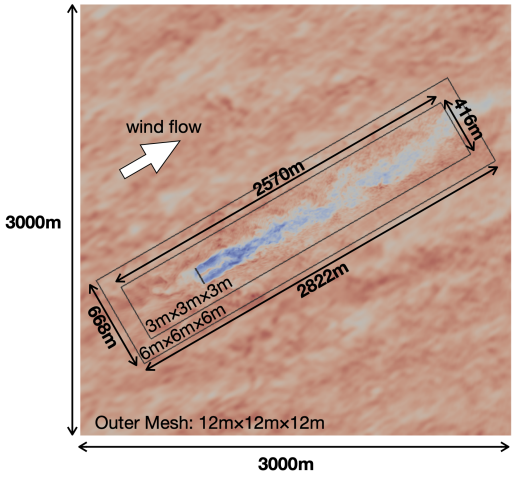

Figure 2. The illustration of the large eddy simulations of wind turbine wakes.

with the actuator line method in the simulations. The computational domain and the mesh configuration are illustrated in Figure 2, where the mean wind direction is southwest. To save the computational resources while ensuring that the detailed wake dynamics are captured, the mesh is generated with three layers of resolutions [34]. A mesh size of 12 m is used in the freestream region, a mesh size of 3 m is used in the wake region, and a mesh size of 6 m is used between the two regions. The wind speeds projected in the laser beam direction at sparse locations are then extracted from the numerical simulations as the measurements by the virtual Lidar device, which is the only training data used for the wind field reconstruction. The full flow field is saved only to serve as the ground truth for performance evaluations.

3. Results

The reconstruction results are given in this section. First, the reconstruction error is reported for a set of NN structures. Then the structure with the best performance is used for the subsequent flow field visualisation and wake analysis.

3.1. Neural network structure

The training is carried out using the Adam optimizer with a learning rate of 10^{-3}. All the data obtained from the virtual Lidar device during the considered time period of 80 seconds is fed into the machine learning model at each training iteration. Thus N_1 in Equation (3) is equal to 16×241. As for the NS test points in the hub-height 2D plane, a batch size of 4000 is used, i.e. N_2 in Equation (4) is equal to 4000.

To tune the NN structure, an error metric needs to be defined to evaluate the accuracy of the reconstructed wind fields. It is defined in this work as the time-averaged value of the root mean square errors (RMSE) of the flow fields, which is expressed as

$$\epsilon_q = \frac{1}{N_t} \sum_{t=1}^{N_t} \sqrt{\frac{1}{N_x} \sum_{i=1}^{N_x} (\hat{q}_{i,t} - q_{i,t})^2} \tag{6}$$

where q represents the quantity of interest, N_t is the total number of time instants, N_x is the total number of test points in the flow domain, and $\hat{q}_{i,t}$ and $q_{i,t}$ represent the predicted and the true values of the quantity q at the i^{th} location and t^{th} instant.

To determine the NN structure, a set of hidden layer neuron numbers and numbers of hidden layers are tested, and the corresponding reconstruction errors are calculated after training. The

Table 1. The tuning of the neural network structure. The structure is denoted by the number of hidden layer neurons × the number of hidden layers.

Neural network structure	Speed range [m/s]	ϵ_u [m/s]	ϵ_u/range
32×3	[1.90, 10.2]	0.858	10.3%
32×5	[1.90, 10.2]	0.890	10.7%
64×3	[1.90, 10.2]	0.916	11.0%
64×5	[1.90, 10.2]	0.824	9.93%
128×3	[1.90, 10.2]	0.835	10.1%
128×5	[1.90, 10.2]	0.752	9.06%

results are given in Table 1. As shown, the best reconstruction performance is achieved with a neural network of 5 hidden layers and 128 neuron numbers. It is therefore used in the rest part of this paper.

3.2. Flow field reconstruction

This section presents the comparison of the reconstructed flow fields with the ground truth. The reconstructed flow field, the ground truth, and their difference are shown from the left to the right side in Figure 3. The results at seven different time instants are included in Figure 3 and each row represents the flow field at one time instant.

As shown, the reconstructed flow fields agree with the ground truth quite well. Particularly, in the near wake and far wake regions, the reconstruction errors remain small. On the other hand, at the side of the turbine where all the Lidar measurement points are far away from this region, the flow information is not well reconstructed. Moreover, when comparing the results at different time instants, as can be seen from different rows of Figure 3, the dynamic characteristics are captured in the reconstructed flow fields, including both the downwind propagation and the crosswind meandering of the flow structures. For example, a low-speed flow structure in the far wake is observed at around [x,y] = [350m, 30m] and at t = 10s, as shown in the first row of Figure 3. Its downwind and crosswind evolution is successfully captured by the reconstructed flow fields, which can be seen from the second to fifth rows of Figure 3. In terms of RMSEs, it was only 0.752 m/s, which is just 9.06% of the value range of the wind field.

3.3. Wake profile prediction

To further showcase the performance of the reconstruction method in capturing wake features, the wake profiles at various downwind stations are extracted from the reconstructed flow fields and then compared with the ground truth. The results are given in Figure 4, where each subfigure includes the velocity profiles from the turbine location (i.e. X = 0D), the near wake region (i.e. X = 1D, 2D, 3D), and to the far wake region (i.e. X = 4D, 5D). The wake profiles at seven different time instants are given, which correspond to the same time instants as in Figure 3. From the extracted wake profiles, it is clearly observed that the wake is induced at the turbine location, then a double peak structure is formed in the near wake region, and finally a single peak structure is observed towards the far wake region. Along with the evolving wake shape, the wake also gradually recovers towards the freestream wind speed. All these essential features are captured by the reconstructed profiles. Aside from the region in the immediate vicinity of the wind turbine, the reconstructed velocity profiles agree well with the corresponding true values. It is worth mentioning that the successful capturing of the double-peak wake structure lies in that the sparse data from the scanning Lidar contains useful information regarding the wake structures while the missing information is retrieved via the flow physics incorporated.

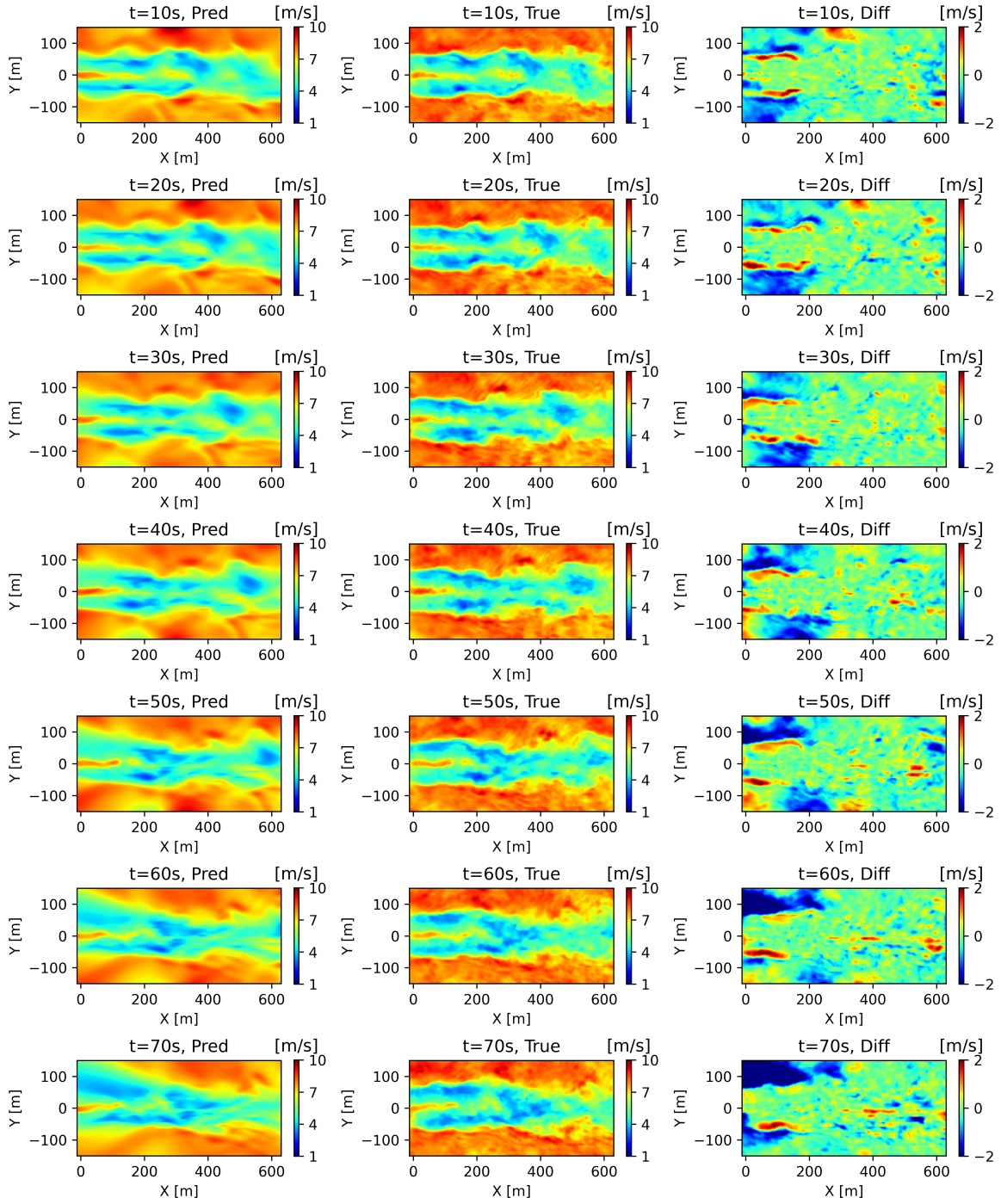

Figure 3. The flow field reconstruction results. The reconstructed flow field, the ground truth, and their difference are shown from the left to the right.

Next, the time-averaged wake profiles are examined for completeness, as most of the previous Lidar-based flow reconstruction focuses on time-averaged wind flow. The results are given in Figure 5. As shown, the averaged wake profiles are predicted very accurately compared with the ground truth. As expected, when compared with the instantaneous flow profiles, a much

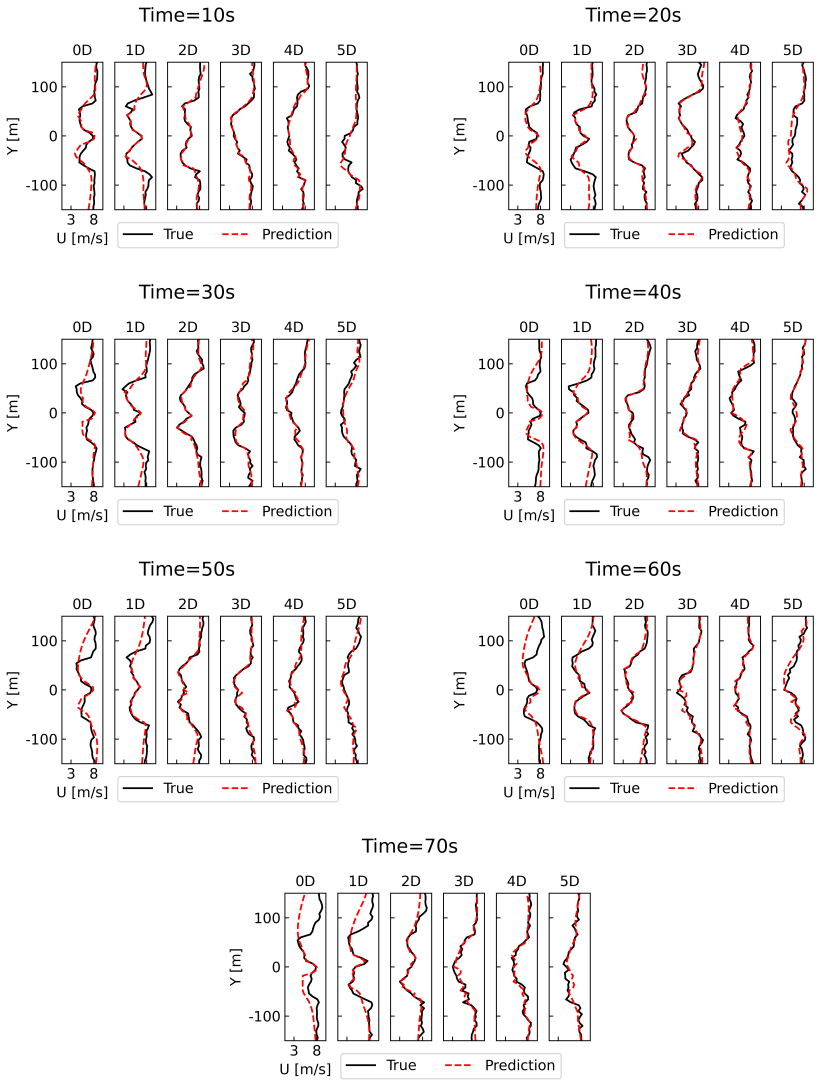

Figure 4. The wake profiles at various downwind stations.

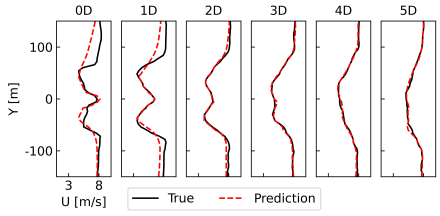

Figure 5. The time-averaged wake profiles at various downwind stations.

smoother profile is observed for the mean profile, which evolves, at the far wake region, into a Gaussian-like profile.

3.4. Effective wind speed prediction

Finally, based on the reconstructed flow fields, the effective wind speed along the downwind direction is extracted. The results, along with the corresponding ground truth, are given in Figure 6. Here the effective wind speed is calculated as the wind speed averaged over the width

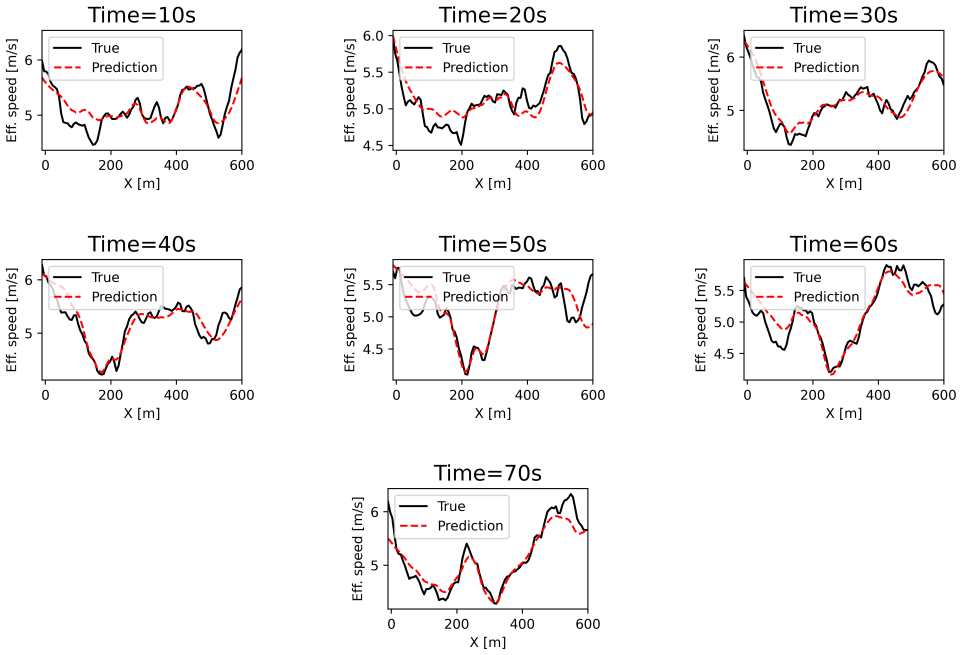

Figure 6. The effective wind speed at various downwind locations and time instants.

of the wind turbine. As shown, the predicted effective wind speeds agree with the true values at different time instants and locations. Particularly, the wind speed reduction due to the presence of the wind turbine, as shown from the turbine location to about 200 m downstream, and the wind speed recovery afterwards, are both captured by the predicted effective wind speed. This accurate prediction of the effective wind speed is a useful example showing the potential use of the reconstructed flow fields for characterizing the wake-induced wind turbine power loss in wind farms.

4. Conclusions

In this work, the reconstruction of the wind turbine wake flow field was investigated, combining a virtual Lidar measurements with two-dimensional Navier-Stokes equations via the physics-informed neural networks. The results showed that the unsteady wake flow fields, including the shape and strength of the wake, were successfully reconstructed, and the main dynamics were well captured. The essential wake features were accurately predicted in the reconstructed wake profiles, including the double peak structure formed in the near wake region and its development towards the single peak structure in the far wake region. The reconstruction error was quantified using the root mean squared error between the predicted and true flow fields. The prediction error was only 0.752 m/s for the wind speed in the inflow wind direction. The successful prediction of the wake deficit and the wake shape indicates the potential use of the reconstructed flow fields for wake analysis in real-world wind energy sites, to assist the understanding and characterisation of full-scale wake flows.

However, the present work combines a virutal Lidar device that is assumed to measure the line-of-sight wind speed without measurement noise. In practice, various error sources for Lidar measurements, such as range weighting (which also increases with the measurement distance), the view blocking of the laser beam by the rotating turbine blades, and the lack of aerosol particles for effective measurements with a valid carrier-to-noise ratio, will affect the quality of the reconstructed flow fields. Therefore, future works will need to take these measurement

errors into account for more realistic evaluations, such as through Bayesian neural networks. In our future work, the investigation of the flow reconstruction performance via wind tunnel experiments, as well as the full-scale field campaign, will be further carried out for validations. In terms of method development, interesting directions include the design of novel approaches to tackle spectral bias to enable efficient training, and the design of effective transfer learning approaches to enable online applications.

Acknowledgments

This work has received funding from the European Union's Horizon Europe Research and Innovation Actions under the grant agreement No 101122329 and the UKRI Horizon Europe Guarantee scheme under the grant No 10095874. The authors also acknowledge the Scientific Computing Research Technology Platform (SCRTP) at the University of Warwick for providing High-Performance Computing resources.

References

[1] Blondel F and Cathelain M 2020 *Wind Energy Science Discussions* **2020** 1–16
[2] Brogna R, Feng J, Sørensen J N, Shen W Z and Porté-Agel F 2020 *Applied energy* **259** 114189
[3] Vahidi D and Porté-Agel F 2022 *Journal of Fluid Mechanics* **943** A49
[4] Bastankhah M, Shapiro C R, Shamsoddin S, Gayme D F and Meneveau C 2022 *Journal of Fluid Mechanics* **933** A2
[5] Ti Z, Deng X W and Yang H 2020 *Applied Energy* **257** 114025
[6] Zhang J and Zhao X 2020 *Applied Energy* **277** 115552
[7] Li S, Zhang M and Piggott M D 2023 *Applied Energy* **339** 120928
[8] Martínez-Tossas L A and Meneveau C 2019 *Journal of Fluid Mechanics* **863** 269–292
[9] Revaz T and Porté-Agel F 2021 *Energies* **14** 3745
[10] Steiner J, Dwight R P and Viré A 2022 *Computers & Fluids* **233** 105213
[11] Iungo G V 2016 *Journal of Wind Engineering and Industrial Aerodynamics* **149** 35–39
[12] Campagnolo F, Weber R, Schreiber J and Bottasso C L 2020 *Wind Energy Science Discussions* **2020** 1–33
[13] Neunaber I, Hölling M, Whale J and Peinke J 2021 *Renewable Energy* **179** 1650–1662
[14] Garcia E T, Aubrun S, Coupiac O, Girard N and Boquet M 2019 *Renewable energy* **130** 1–11
[15] Zhan L, Letizia S and Valerio Iungo G 2020 *Wind Energy* **23** 501–527
[16] Letizia S, Zhan L and Iungo G V 2021 *Atmospheric Measurement Techniques* **14** 2095–2113
[17] Schneemann J, Theuer F, Rott A, Dörenkämper M and Kühn M 2020 *Wind Energy Science Discussions* **2020** 1–26
[18] Kelberlau F, Neshaug V, Lønseth L, Bracchi T and Mann J 2020 *Remote Sensing* **12** 898
[19] Cañadillas B, Beckenbauer M, Trujillo J J, Dörenkämper M, Foreman R, Neumann T and Lampert A 2022 *Wind Energy Science* **7** 1241–1262
[20] Van Dooren M F, Trabucchi D and Kühn M 2016 *Remote Sensing* **8** 809
[21] Carbajo Fuertes F and Porté-Agel F 2018 *Remote Sensing* **10** 721
[22] Beck H and Kühn M 2019 *Remote Sensing* **11** 2665
[23] Conti D, Pettas V, Dimitrov N and Peña A 2021 *Wind Energy Science* **6** 841–866
[24] Raissi M, Perdikaris P and Karniadakis G E 2019 *Journal of Computational physics* **378** 686–707
[25] Raissi M, Yazdani A and Karniadakis G E 2020 *Science* **367** 1026–1030
[26] Cai S, Li H, Zheng F, Kong F, Dao M, Karniadakis G E and Suresh S 2021 *Proceedings of the National Academy of Sciences* **118** e2100697118
[27] Zhang J and Zhao X 2021 *Applied Energy* **288** 116641
[28] Zhang J and Zhao X 2021 *Applied Energy* **300** 117390
[29] Zhang J and Zhao X 2023 *Energy Conversion and Management* **293** 117507
[30] 2024 ZXLidars Product Guide https://www.zxlidars.com
[31] Churchfield M and Lee S 2012 Nwtc information portal (sowfa). https://nwtc.nrel.gov/sowfa
[32] Churchfield M J, Lee S, Michalakes J and Moriarty P J 2012 *Journal of turbulence* N14
[33] Jonkman J, Butterfield S, Musial W and Scott G 2009 Definition of a 5-mw reference wind turbine for offshore system development Tech. rep. National Renewable Energy Lab.(NREL), Golden, CO (United States)
[34] Fleming P, Gebraad P M, Lee S, van Wingerden J W, Johnson K, Churchfield M, Michalakes J, Spalart P and Moriarty P 2015 *Wind Energy* **18** 2135–2143